Journal
of the American Ceramic Society

Long-term ceramic reliability analysis including the crack-velocity threshold and the "bathtub" curve

Robert F. Cook[1] (iD)

Materials Measurement Science Division, National Institute of Standards and Technology, Gaithersburg, Maryland

Correspondence
Robert F. Cook, Materials Measurement Science Division, National Institute of Standards and Technology, Gaithersburg, MD.
Email: robert.cook@nist.gov

Abstract

A thermally activated crack-velocity formulation that includes a threshold at thermodynamic equilibrium is used in the prediction of long-term time-to-failure for brittle materials. A new closed-form time-to-failure solution is derived for straight cracks propagating under the influence of constant stress. Explicit connections are made between the macroscopic crack-velocity parameters and the underlying bond-rupture parameters. A feature of the solution is the divergence of time-to-failure for applied loading approaching the thermodynamic threshold. A new reliability framework is developed and long-term reliability and hazard predictions made using the time-to-failure solution. A bathtub hazard curve is shown to be generated by a single crack-velocity failure mechanism.

KEYWORDS
applications, brittle materials, crack velocity, cracks/cracking, mechanical properties

1 | INTRODUCTION

Many works have demonstrated a crack-velocity formulation derived from the fundamental kinetics of bond rupture in describing reactive fracture processes in ceramics—including crack initiation and propagation[1–3] and component failure.[1,4,5] The formulation is based on 2 principles:[6] (i) that there exists in the ceramic a periodic array of barriers to crack propagation, which are overcome by thermal activation; and (ii) that the barriers are biased in favor of forward or backward crack motion by the mechanical energy release rate associated with stress fields in the cracked material. If the stresses bias the system in favor of forward crack motion and the thermal activation is great enough, then the component will eventually fail—the time-to-failure is related to both the crack-propagation kinetics and the stresses. If the stresses bias forward and backward crack motion equally, then crack propagation is zero, the component is at the crack-velocity threshold and never fails—the time-to-failure diverges. Specification of the complete stress dependence for time-to-failure of a component is critical in predicting reliability (the probability that a ceramic component will survive as a function of time). Long-term, near

divergent, time-to-failure reliability predictions require clear specification of threshold effects. Successful as the bond-rupture-based formulation has been in describing reactive fracture,[2,5] there appears to be no published analytical solution for time-to-failure including the crack-velocity threshold, and, consequently, there is no long-term ceramic reliability methodology. Both these issues are addressed here.

First, thermally activated cracking and failure is considered and the required analytical solution for time-to-failure is developed. The solution permits clear examination of the effects of the macroscopic crack-velocity parameters, including the threshold, and, alternatively, the effects of the related nanoscale bond-rupture parameters. A reliability formulation is then developed and the relationship between component reliability and strength distribution examined in the context of the time-to-failure solution. The formulation uses concepts for analysis of ceramic reliability, advocated previously,[7] which although long accepted in considering semiconductor reliability have been little used in consideration of lifetimes of structural ceramics. Finally, the conditions under which a population of ceramic components exhibit the extremely common "bathtub" reliability

response is examined. A bathtub response includes an initial, short-term decrease in relative failure rate, followed by a period of constant relative failure rate, and finally, in the long term, an increase in relative failure rate.[7–9] The full relative failure rate, also known as the hazard response, thus resembles the cross-section of a bathtub and prediction requires the specification of the full time-to-failure behavior of a material. Appendices 1 and 2 detail the connections of the present work to previous, popular crack-velocity formulations.

2 | CRACK PROPAGATION AND FAILURE TIME ANALYSIS

2.1 | Crack velocity

Consideration of the mechanical and surface energy changes during crack advance shows that the areal crack expansion rate $\dot{A}$ is,[2]

$$\dot{A} = \dot{A}_0 \sinh\left[\frac{(G - 2\gamma)}{\eta}\right], \qquad (1)$$

where G is the mechanical energy release rate, and,

$$\begin{aligned}
\eta &= \frac{2kT}{a^2} \\
2\gamma &= \frac{u_0}{a^2} \\
\dot{A}_0 &= 2f_0 a^2 \exp\left(\frac{-u_1}{kT}\right)
\end{aligned} \qquad (2)$$

The terms on the right sides are related to the periodic atomistic potential in a solid, U_S, characterizing the energy barriers to create new surface:

$$U_S = u_0\left(\frac{A}{a^2}\right) - \left(\frac{u_1}{2}\right)\cos\left(\frac{2\pi A}{a^2}\right), \qquad (3)$$

where A is the crack area and a^2 is the incremental "bond" area—the average spatial separation between the barriers to bond rupture is a. Equation 2 shows that the macroscopic crack-velocity parameter η is a measure of the average thermal energy per bond (k = Boltzmann's constant, T = temperature). $f_0 = kT/h$ (h = Planck's constant) is a characteristic frequency. The energy to break a bond and create an incremental area a^2 of equilibrium surface in the test environment is u_0 (Equation 3). For a bond-rupture reaction $x\mathbf{E} + \mathbf{F} \rightarrow \mathbf{F^*}$, where $\mathbf{E}$ represents an environmental species, $\mathbf{F}$ represents an intact bond, and $\mathbf{F^*}$ represents an equilibrium fractured bond pair, u_0 is related to the difference in the appropriate chemical potentials by $u_0 = \mu_{\mathbf{F^*}} - \mu_{\mathbf{F}} - x\mu_{\mathbf{E}}$. The macroscopic quantity 2γ is then the "surface energy." (In an *inert* environment, $x\mu_{\mathbf{E}} = 0$ and 2γ takes the maximum value of $2\gamma_0$, considered below.) For $G = 2\gamma$, the fracture system is in reactive

equilibrium and the crack expansion rate is zero, as required thermodynamically.[10] The ratio $W = 2\gamma/\eta = u_0/2kT$ is an important measure of the relative chemical and thermal energies in the system: For large W, fracture is chemically dominated; for small W, fracture is thermally dominated.

In equilibrium, bond rupture and bond healing states are separated by energy barriers of magnitude u_1. The local metastable and unstable equilibrium points are displaced $-u_1/2$ and $+u_1/2$, respectively, from the arbitrary zero of surface potential in Equation 3. It is the necessity of thermal activation over these energy barriers that depresses the characteristic frequency of motion from one metastable state to the next, from f_0 to modification by the Arrhenius term in Equation 2. The macroscopic quantity $\dot{A}_0$ is then seen as a characteristic crack expansion rate, and the overall rate in Equation 1 as the product of this kinetic term and a function of the displacement of the system from thermodynamic equilibrium, $G - 2\gamma$. Alternative expressions based on different physical principles, not without debate, are related to the current work in Appendix 1.

For a crack characterized by a single geometrical parameter c, the area A and crack length c are related by[11] $A = \alpha_S c^D$, where D is the number of dimensions in which the crack is extending and α_S is a geometrical prefactor (eg, $\alpha_S = w$ and $D = 1$ for a straight crack extending in a component of width w and $\alpha_S = \pi$ and $D = 2$ for a circular crack). The crack velocity v along the dimension c is

$$v = \frac{dc}{dt} = \frac{dA}{dt} \cdot \frac{dc}{dA},$$

and hence from Equation 1,

$$v = \left(\frac{adc}{dA}\right)v_0 \sinh\left[\frac{(G - 2\gamma)}{\eta}\right],$$

where using Equation 2, v_0 is a material-dependent, geometry-independent characteristic velocity,

$$v_0 = 2af_0\exp\left(\frac{-u_1}{kT}\right), \qquad (4)$$

This definition of v_0 excludes all geometry dependence—preserving the trio (η, 2γ, v_0) as material-only parameters.[5] The definition also emphasizes the strong dependence that any observed $v(G)$ behavior has on system geometry through the adc/dA term, and that this term is *only* independent of crack length for linear $D = 1$ systems. Writing $B = dA/adc$ gives the crack velocity generally as

$$v = v_0 \sinh\frac{[(G - 2\gamma)/\eta]}{B}, \qquad (5)$$

where $B = s/a$ is the ratio of the lengths of the instantaneous crack periphery s and the lattice period (eg, $s = w$

for a straight crack in a component of width w, $s = 2\pi c$ for a circular crack of radius c). B gives the number of active sites on the crack front. Equation 5 reduces in the forward-activation limit of $G \gg 2\gamma$ to,

$$v = v_A \exp\left(\frac{G}{\eta}\right), \tag{6}$$

where $v_A = (v_0/2B)\exp(-2\gamma/\eta)$ contains information about the threshold.

Once a set of $(\eta, 2\gamma, v_0)$ is determined for a given system, the inverse relations,

$$
\begin{aligned}
a &= \left(\frac{2kT}{\eta}\right)^{1/2} \\
u_0 &= 2\gamma a^2 \\
u_1 &= kT\ln\left(\frac{2akT}{v_0 h}\right)
\end{aligned}
\tag{7}
$$

give the invariant parameters characterizing the lattice potential, Equation 3, for that material and environment. On a $v(G)$ plot (with G as the abscissa), 2γ is a measure of the horizontal position, v_0 is a measure of the vertical position, and $1/\eta$ is a measure of the slope in the forward-activation-dominated region.[4] The transformation relations of Equations 2, 4, and 7 show that the atomistic bond-rupture parameters are reflected in these changes by u_0 affecting the horizontal position, u_1 affecting the vertical position, and a influencing vertical and horizontal positions and slope. For a given material-environment combination, that is, the set of (a, u_0, u_1) all fixed, increasing temperature causes upward vertical shifts and decreases the slope.[2] Figures 1 and 2 show the effects of variations in the macroscopic and atomistic parameters on $v(G)$ curves, using Equation 5. As a practical matter, the set of atomistic parameters (a, u_0, u_1) is most easily determined by fitting macroscopic crack velocity[2,6] or time-to-failure responses.[4,5] Scaling of the parameters between materials is possible by independent models.[3]
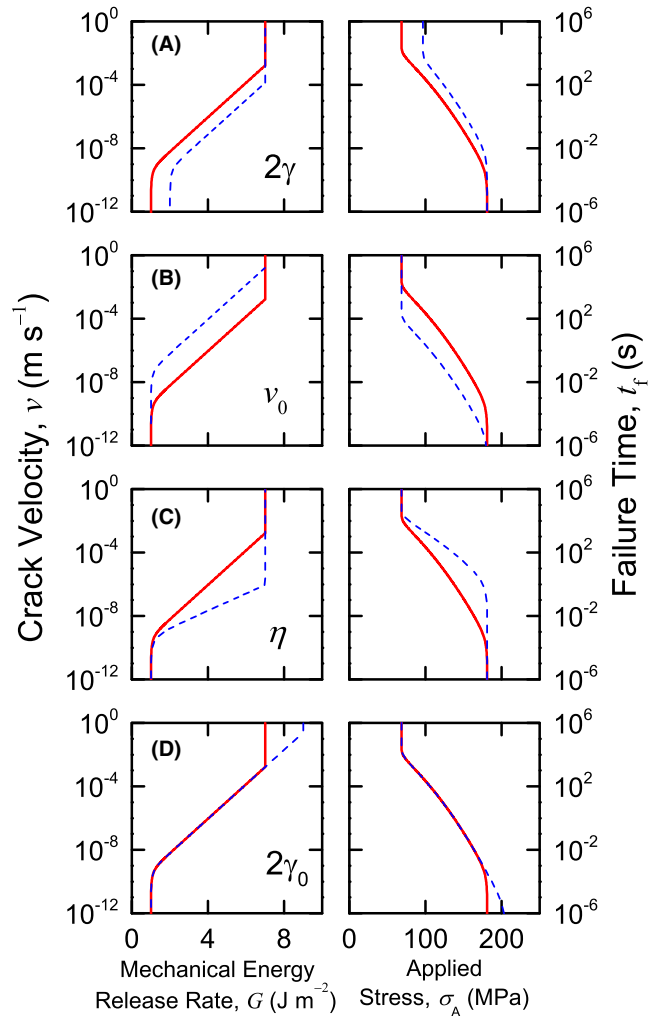
2.2 | Time-to-failure

Analytic solutions are possible for time-dependent crack growth and failure for a straight crack in a uniform, constant, applied stress field. Under such conditions G is given by,

$$G = \Sigma c, \tag{8a}$$

where

$$\Sigma = \frac{\psi^2 \sigma_A^2}{E^*}, \tag{8b}$$

σ_A is the constant applied stress, E^* is a material modulus, and ψ is a dimensionless geometry term. For a crack of

FIGURE 1 Plots showing altered macroscopic variables in crack-velocity $v(G)$ curves and resulting time-to-failure $t_f (\sigma_A)$ responses. The solid line is common to each plot with $2\gamma = 1$ J m^{-2}, $v_0 = 10^{-3}$ m s^{-1}, $\eta = 0.4$ J m^{-2}, and $2\gamma_0 = 7$ J m^{-2}. Dashed lines are increases of (A) 2γ to 2 J m^{-2}; (B) v_0 to 10^{-1} m s^{-1}; (C) η to 0.8 J m^{-2}; and (D) $2\gamma_0$ to 9 J m^{-2}. Other parameters are $B = 10^6$ and $c_0 = 10$ μm [Color figure can be viewed at wileyonlinelibrary.com]

initial length c_0, the time t_c taken to extend the crack to length c from c_0, combining Equations 5 and 8a and integrating (for a straight crack, B is invariant) is as follows:

$$t_c = \int_0^{t_c} dt = \int_{c_0}^{c} \frac{dc'}{v_0 \sinh[(\Sigma c' - 2\gamma)/\eta]/B}. \tag{9}$$

As the crack velocity is only a function of the departure of the system from equilibrium, it is convenient to change the variable of integration to reflect this. Setting,

$$z = \frac{(\Sigma c - 2\gamma)}{\eta}, \tag{10}$$

gives Equation 9 as
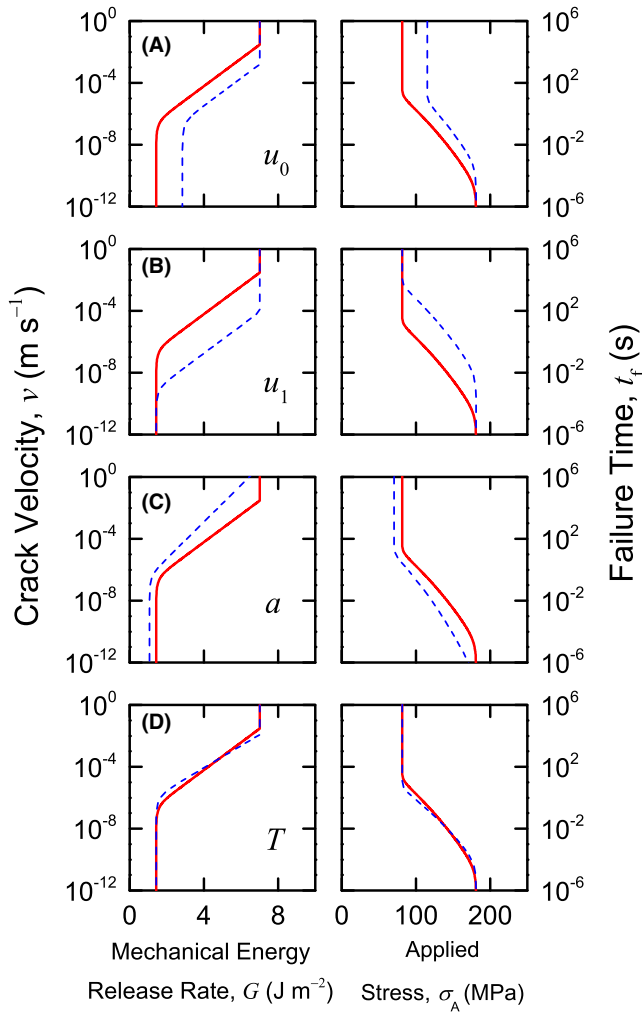
FIGURE 2 Plots showing altered atomistic variables in crack-velocity $v(G)$ curves and resulting time-to-failure t_f (σ_A) responses. The solid line is common to each plot with $u_0 = 0.15$ eV (1 eV = 1.6×10^{-19} J), $u_1 = 0.15$ eV, $a = 0.13$ nm, and $T = 25°C$. Dashed lines are increases of (A) u_0 to 0.3 eV; (B) u_1 to 0.3 eV; (C) a to 0.15 nm; and (D) T to 100°C. Other parameters are $2\gamma_0 = 7$ J m^{-2}, $w = 1$ mm, and $c_0 = 10$ μm [Color figure can be viewed at wileyonlinelibrary.com]

$$t_c = \frac{\eta B}{\Sigma v_0} \int_{z_0}^{z} \frac{dz'}{\sinh(z')}$$
$$= \frac{\eta B}{\Sigma v_0} \left[\ln\left(\tanh\left(\frac{z'}{2} \right) \right) \right]_{z_0}^{z}. \qquad (11)$$
$$= \frac{\eta B}{\Sigma v_0} \ln\left(\frac{e^z - 1}{e^z + 1} \cdot \frac{e^{z_0} + 1}{e^{z_0} - 1} \right)$$

In re-expressing z in terms of c, it is convenient to recognize that there are upper and lower bounds to the applied stress within which time-dependent crack extension and hence time-dependent failure occur: $\sigma_{max} \geq \sigma_A \geq \sigma_{min}$. The upper bound, σ_{max}, is the familiar Griffith specification[12] of the applied stress necessary to attain equilibrium for a cracked material in an inert environment ($x\mu_E = 0$ above). For a crack of length c_0, this stress is given by

$$\Sigma_{max}c_0 = 2\gamma_0, \qquad (12a)$$

where

$$\Sigma_{max} = \frac{\psi^2 \sigma_{max}^2}{E^*}. \qquad (12b)$$

The analogous lower bound, σ_{min}, is the Orowan specification[13] of the applied stress necessary to attain equilibrium for a cracked material in a reactive environment ($x\mu_E \neq 0$). For a crack of length c_0, this stress is given by

$$\Sigma_{min}c_0 = 2\gamma, \qquad (13a)$$

where

$$\Sigma_{min} = \frac{\psi^2 \sigma_{min}^2}{E^*}. \qquad (13b)$$

Both equilibria are unstable as $dG/dc > 0$, Equation 8a, such that any positive perturbation from equilibrium leads to crack extension. In the inert case, the crack propagation is dynamic and component failure almost instantaneous; this is the failure condition to be considered below. In the reactive case, the crack propagation is kinetically limited and component failure is time dependent; this is the immediate concern.

Figure 3A shows a diagram of G vs c in logarithmic coordinates for constant applied stress loading. The initial crack length c_0 is shown as the dashed vertical line, and the equilibrium surface energies $2\gamma_0$ and 2γ are shown as the dashed horizontal lines. $(c_0, 2\gamma_0)$ and $(c_0, 2\gamma)$ are points of inert and reactive unstable equilibrium, respectively; the solid diagonal lines passing through these points represent the $G(c)$ trajectories for the Griffith and Orowan strength limits, σ_{max} and σ_{min}. Figure 3B is a similar diagram with identical dashed lines, including the Griffith and Orowan trajectories. The point $(c_0, 2\gamma + z_0\eta)$ represents a system initially perturbed to a nonequilibrium reactive position by an increase in G of $z_0\eta$; crack extension thence proceeds along the $G(c)$ trajectory defined by σ_A, shown as the solid diagonal line. Using Equation 13a, the general displacement from equilibrium along the trajectory can be expressed as follows:

$$z = \frac{2\gamma}{\eta} \left(\frac{\Sigma c}{\Sigma_{min}c_0} - 1 \right), \qquad (14a)$$
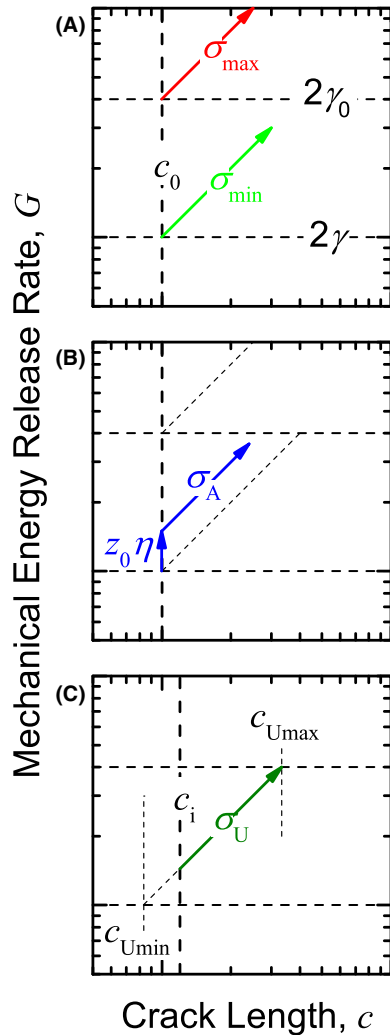
and the initial perturbation as

$$z_0 = \frac{2\gamma}{\eta} \left(\frac{\Sigma}{\Sigma_{min}} - 1 \right). \qquad (14b)$$

Using Equation 8b to set,

$$S^2 = \frac{\Sigma}{\Sigma_{min}} = \frac{\sigma_A^2}{\sigma_{min}^2}$$
$$C = \frac{c}{c_0} \qquad , \qquad (15)$$
$$T_C = \frac{t_c v_0}{c_0}$$

yields the normalized time T_C for relative crack extension C as

FIGURE 3 Plots of mechanical energy release rate G vs crack length c for a solid under uniform applied stress. The horizontal dashed lines indicate equilibrium surface energies, the vertical dashed lines indicate initial crack lengths, and the solid lines indicate nonequilibrium system trajectories. (A) The bounding inert (σ_{max}) and reactive (σ_{min}) trajectories for a crack length c_0. (B) The crack propagation trajectory for a system with crack length c_0 perturbed by stress σ_A. (C) The bounding minimum ($c_{U_{min}}$) and maximum ($c_{U_{max}}$) crack lengths for crack propagation under stress σ_U, along with the failure trajectory from a crack length c_i [Color figure can be viewed at wileyonlinelibrary.com]

$$T_C = \frac{B}{WS^2} \ln\left(\frac{e^{W(S^2C-1)} - 1}{e^{W(S^2C-1)} + 1} \cdot \frac{e^{W(S^2-1)} + 1}{e^{W(S^2-1)} - 1}\right), \quad (16a)$$

after combining Equations 14 and 15 into Equation 11, noting, as anticipated, the central role of the ratio W. Equation 16a gives the time required to proceed along the reactive $G(c)$ trajectory shown in Figure 3B.

The general condition for component failure and the termination of the trajectory in Figure 3B is that the crack length reach a relative extension C_f, such that the time-to-failure, T_f, is given by simple modification of Equation 16a:

$$T_f = \frac{B}{WS^2} \ln\left(\frac{e^{W(S^2C_f-1)} - 1}{e^{W(S^2C_f-1)} + 1} \cdot \frac{e^{W(S^2-1)} + 1}{e^{W(S^2-1)} - 1}\right), \quad (16b)$$

C_f could be a critical component dimension or compliance factor, or specify a condition for crack bifurcation, for instance. The traditional criterion for failure, and the one used here, is that $G = 2\gamma_0$ as it allows for explicit connection with the inert strength, σ_{max}. Using Equation 8a, an unstable inert equilibrium point is defined along the reactive trajectory by $(c_f, 2\gamma_0)$, Figure 3B, such that,

$$2\gamma_0 = \Sigma c_f (= \Sigma_{max} c_0). \quad (17)$$

Extending Equation 15 by

$$S_{max}^2 = \frac{\Sigma_{max}}{\Sigma_{min}} = \frac{\sigma_{max}^2}{\sigma_{min}^2} = S^2 C_f, \quad (18)$$

allows the elimination of the crack length from Equation 16b by the inert strength and hence,

$$T_f = \frac{B}{WS^2} \ln\left(\frac{e^{W(S_{max}^2-1)} - 1}{e^{W(S_{max}^2-1)} + 1} \cdot \frac{e^{W(S^2-1)} + 1}{e^{W(S^2-1)} - 1}\right). \quad (19)$$

Equation 19 includes 3 asymptotic responses:

$$S \to 1, T_f \to \infty$$
$$1 \ll S \ll S_{max}, T_f \to 2Be^{-W(S^2-1)}/WS^2. \quad (20)$$
$$S \to S_{max}, T \to 0$$

(using $\ln[(x + 1)/(x - 1)] = 2(1/x + \dots)$ for $x \gg 1$ for the central asymptote). Figure 4 shows the increased time-to-failure with decreasing applied stress from Equation 19 as the solid line (this and all subsequent figures are in normalized coordinates). The asymptotes of Equation 20 are shown as the dashed lines; the central asymptote is shown as the diagonal dashed line and can be obtained by integrating Equation 6 directly. For a system perturbed a long way from either equilibrium state, such approximated solutions often
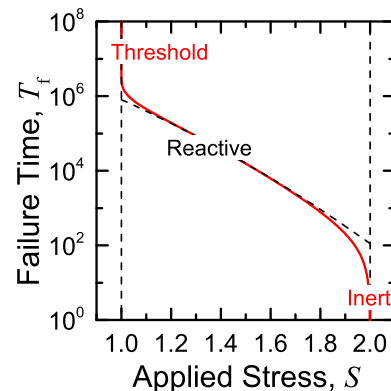
FIGURE 4 Plot of normalized time-to-failure vs normalized applied stress, T_f vs S, for a material with inert strength $S_{max} = 2$. Geometry and surface/thermal energy parameters are $B = 10^6$ and $W = 2.5$ [Color figure can be viewed at wileyonlinelibrary.com]

form the basis for "exact" inversion of $t_f(\sigma_A)$ data to $v(G)$ data—especially for power-law approximations to $v(G)$.[14] Appendix 2 contains lifetime solutions analogous to those above for a power-law approximation to the $v(G)$ curve that includes a threshold. Figures 1 and 2 show the effects of changing the macroscopic and atomistic $v(G)$ parameters on $t_f(\sigma_a)$ curves, using Equation 19 and the transformation Equations 2, 7, 12, 13, and 15. Time-to-failure responses are seen to be inverted, slightly curved, and "smoothed" versions of crack-velocity curves.

3 | RELIABILITY ANALYSIS

3.1 | Unimodal crack populations

The above formulation provides *scientific* insight, relating component time-to-failure to the fundamental parameters of the bond-rupture kinetics. *Engineering* insight is provided by using the results of this formulation to relate a distribution of crack lengths set by the manufacturing process to subsequent component reliability in use. The first step in developing a reliability framework is to recognize that the variables crack length, strength, and stress used above need to be rearranged. In the above, a crack length was assumed, providing strength limits, and the time-to-failure calculated as a function of applied stress. In making a reliability prediction, the applied stress is the use stress and known or assumed, providing crack-length limits, and a distribution of failure times is calculated as function of the distribution of crack lengths within these limits set by the manufacturing process.

If σ_U is the (constant) use stress, a minimum crack length is set by

$$c_{U_{min}} = \frac{2\gamma}{\Sigma_U},\tag{21a}$$

where

$$\Sigma_U = \frac{\psi^2 \sigma_U^2}{E^*}.\tag{21b}$$

in analogy with Equation 13. This is the minimum length for crack propagation set by reactive equilibrium at the use stress. Similarly, a maximum crack length is set by

$$c_{U_{max}} = \frac{2\gamma_0}{\Sigma_U}.\tag{22}$$

This is the maximum length for crack propagation set by inert equilibrium at the use stress. Equations 21 and 22 provide bounds on the initial crack lengths generated by the manufacturing process for which it is meaningful to calculate reliability. Figure 3C is similar to Figures 3A,B and shows $c_{U_{min}}$ and $c_{U_{max}}$ as vertical dashed lines and the $G(c)$ trajectory appropriate to σ_U as the diagonal dashed line. If a crack of initial length c_i is introduced into a component, the system moves along the trajectory from c_i to

failure at $c_{U_{max}}$ as shown by the solid line. All cracks with lengths $c_{U_{min}} \leq c_i \leq c_{U_{max}}$ propagate in the same way and fail at a common failure crack length of $c_{U_{max}}$. Replacing c_0 with $c_{U_{min}}$ in Equation 15, noting that $c_{U_{max}}/c_{U_{min}} = W_0/W$, allows Equation 11 to be re-cast in analogy to Equation 19. Hence (dropping subscripts for simplicity), the time-to-failure T in terms of initial crack length C is

$$T = \frac{B}{W} \ln\left(\frac{e^{W_0-W}-1}{e^{W_0-W}+1} \cdot \frac{e^{WC-W}+1}{e^{WC-W}-1}\right),\tag{23}$$

with bounding asymptotes of $C \to 1$ and $C \to W_0/W$ and intermediate asymptote of,

$$T \to \frac{2Be^{W-WC}}{W}.\tag{24}$$

Equation 23 is the basis for reliability predictions.

The fundamental characteristic of the population of cracks generated by a manufacturing process is the probability density function (pdf) of crack lengths, $f(C)$, here taken to represent a large population and therefore expressed as a continuous function. The pdf here has finite support between population bounds $C_{P_{min}}$ and $C_{P_{max}}$ with $1 \leq C_{P_{min}} \leq C_{P_{max}} \leq W_0/W$ and normalization of,

$$\int_{C_{P_{min}}}^{C_{P_{max}}} f(C)dC = 1.\tag{25}$$

The cumulative distribution function (cdf) is[8]
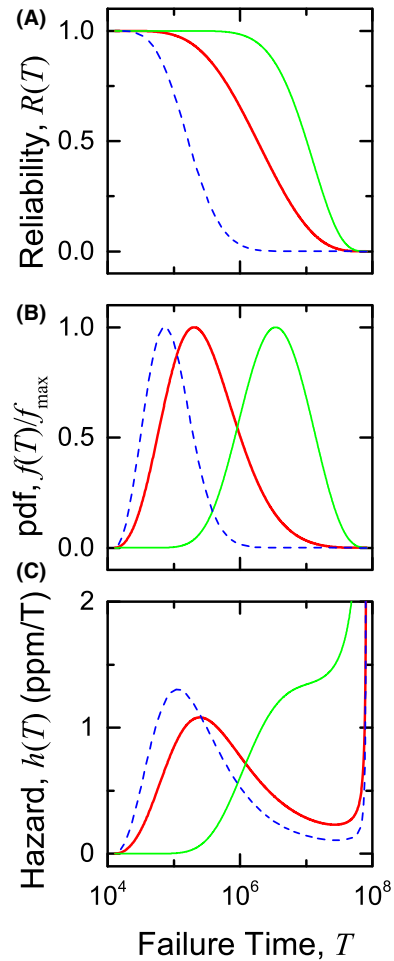
$$F(C) = \int_0^C f(C)dC,\tag{26}$$

and here $F(C \leq C_{P_{min}}) = 0$ and $F(C \geq C_{P_{max}}) = 1$. The probability that a crack selected at random from the population has length less than C is $F(C)$. Figure 5A,B shows the pdf $f(C)$ and cdf $F(C)$ functions, respectively, for 3 populations of cracks with $W_0/W = 4$ and the region of support covering almost the complete allowed domain with $C_{P_{min}} = 1.1$ and $C_{P_{max}} = 3.9$. The pdfs are all unimodal, and thus, the cdfs are all sigmoidal. (Here and throughout, the normalization of Equation 25 is implemented such that only the shape and not numerical magnitude of f is retained. Hence, it is convenient to represent the pdf as f/f_{max}, where f_{max} is the appropriate maximum value (Figures 5-7). In all cases, simple polynomial representations were used for f. The central population (bold lines) is symmetric and the outer populations are skewed to smaller (fine lines) and larger (dashed lines) crack lengths. As the kinetic parameters are fixed, Figure 5C shows the common time-to-failure for all populations from Equation 23 as the solid line. The common bounds on the failure times conjugate to the crack-length bounds, noting the reversals, are $T_{P_{min}} = T(C_{P_{max}}) \approx 10^4$ and $T_{P_{max}} = T(C_{P_{min}}) \approx 10^8$. The intermediate failure time asymptote of Equation 24 is
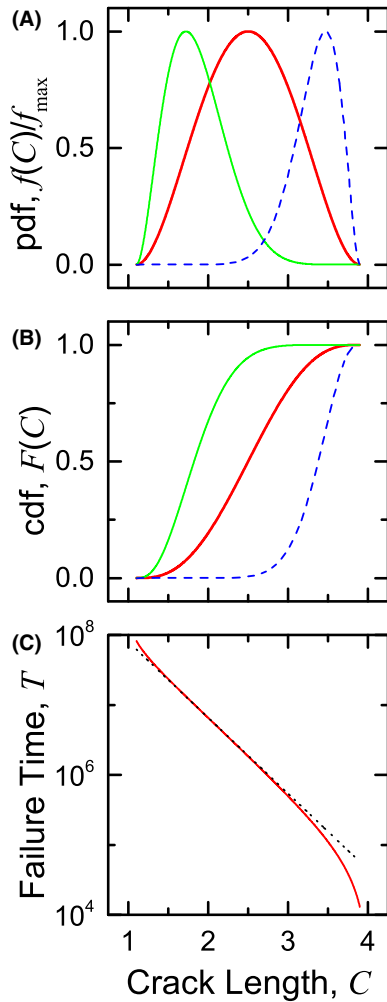
FIGURE 5 (A) Plots of pdf curves for 3 unimodal crack-length populations. (B) Plots of the conjugate sigmoidal cdf curves for the 3 populations. (C) Plot of failure time as a function of crack length using $W_0/W = 4$ [Color figure can be viewed at wileyonlinelibrary.com]

FIGURE 6 (A) Plots of reliability for the 3 populations shown in Figure 5. (B) Plots of failure time pdf curves for 3 crack-length populations. (C) Plots of hazard rate for the 3 populations [Color figure can be viewed at wileyonlinelibrary.com]

shown as the dashed line and describes the response over much of the allowed domain. In this case, threshold and inert strength proximity effects are small.

As noted in Equation 23 and Figure 5C, $dT/dC < 0$, and hence direct replacement of C by T using Equation 23 in $F(C)$ results in the complementary cumulative distribution function (ccdf) of failure times or the *reliability* of the population, $R(T) = 1 - F(T)$.[7–9] The reliability $R(T)$ gives the probability that a crack randomly selected from population will have a time-to-failure greater than T. The bounds of the reliability are $R(T \leq T_{P_{min}}) = 1$ and $R(T \geq T_{P_{max}}) = 0$. Figure 6A combines Figure 5B,C to show the reliability of the 3 unimodal populations. The reliability decreases from 1 (completely reliable) to 0 (guaranteed failure) over the domain of failure time bounds set by the population of crack lengths. The decrease is more rapid for the larger crack-length population. In the semi-logarithmic coordinates used, $R(T)$ curves appear as a reversed versions of

$F(C)$ curves as threshold and inert strength effects are small. Noting that,

$$f(T) = \frac{-dR(T)}{dT}, \quad (27)$$

Figure 6B shows $f(T)$ pdfs of the 3 populations from Figure 5A. Again, in the semi-logarithmic coordinates used, $f(T)$ curves appear as a reversed versions of $f(C)$ curves: long cracks lead to short failure times and vice versa.

The *hazard* of a population gives the relative failure rate, the rate of failure of components relative to the number of intact components. Hazard is the most noticeable factor in component failure and hazard data are easily collected experimentally. Hazard, $h(T)$, is given by the ratio of Equations 26 and 27,[7–9]

$$h(T) = \frac{f(T)}{R(T)}, \quad (28)$$

and is the conditional probability that a crack will fail in the infinitesimal time interval $T + dT$ given that it has not

failed in time T. Figure 6C shows the hazard curves for the 3 unimodal populations. The hazard for the central population increases from 0 to about 1 ppm/T as T increases from $T_{P_{min}}$, and then decreases back to about 0.2 ppm/T at $T \approx 10^7$: the maximum reflects the maximum in the population of failure times (Figure 6B). The hazard then increases dramatically and formally diverges at $T_{P_{max}}$, Equation 28, reflecting the ever-decreasing number of intact components (Figure 6A). The hazard for the large-crack population is similar, although the maximum occurs earlier, reflecting the greater number of shorter failure times. The hazard for the small-crack population is different, remaining close to 0 until $T \approx 10^6$, before increasing to over 1 ppm/T at $T \approx 10^7$ before diverging. Very different experiences of "reliability" would be gained from the 3 populations although they have similar $R(T)$ responses.

3.2 | Bathtub curve

A particularly common form of hazard is the "bathtub" curve, so named after the cross-section of a bathtub.[7,9] Initially, hazard is large and decreases with time and is associated with component "burn-in" or poor-quality control of components with large flaws accidentally put into use. This behavior is then followed by a long period of very small hazard described as "normal" reliability. Finally, the hazard increases and is associated with component "wear-out." Implicit in these terms is that failure in the 3 regions of the curve is caused by different mechanisms. However, it is possible to generate a bathtub curve using a single failure mechanism—nonequilibrium crack propagation—acting on a particular crack population.

Figure 7A shows a tri-modal failure time population pdf consisting of 2 large subpopulations of very short failure times and very long failure times, separated by a small subpopulation of intermediate failure times. The entire population, $f(T)$, is not quite symmetric: The $f(T)$ variation in Figure 7A can be formed by summing the $f(T)$ variations in Figure 6B and normalizing, after asymmetrically shifting the exterior subpopulations to more extreme values and reducing the relative amplitude of the interior subpopulation. The overall population represents a manufacturing process that is dominated by the production of many superior components that fail eventually and perturbed by many inferior components that fail rapidly. Also shown in Figure 7A is the related reliability, $R(T)$, which is dominated by the central near straight-line response of the intermediate subpopulation. Using semi-logarithmic coordinates, the responses appear as reversed from the underlying crack-length populations (not shown). The simple procedure used to generate the $f(T)$ and $R(T)$ curves in Figure 7A leads to radically different curves from those in Figures 5 and 6 with nonzero values across the entire domain and central
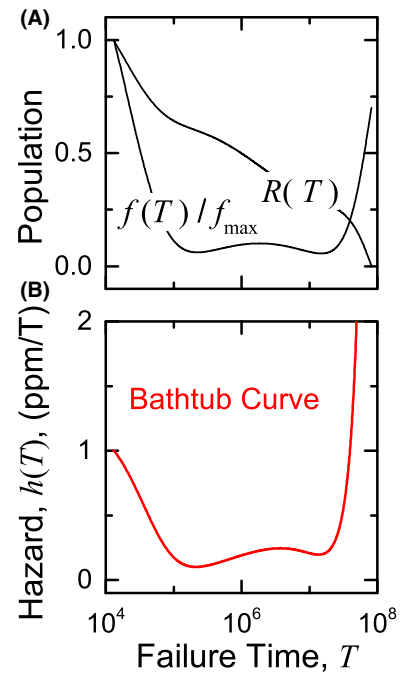
FIGURE 7 (A) Plot of failure time pdf $f(T)$ and conjugate reliability $R(T)$ for a trimodal crack-length population. (B) Plot of the hazard rate for the trimodal population describing a characteristic bathtub curve [Color figure can be viewed at wileyonlinelibrary.com]

minima rather than maxima. Figure 7B shows the resultant hazard response from Figure 7A: it is a bathtub curve, beginning at a nonzero value, decreasing to a long period of near zero, and then ending with an increase. (Note that all hazard curves will show an increase and divergence if the failure time is taken to the maximum bound, as $R(T_{P_{max}}) \rightarrow 0$.) Consideration of Figure 5C shows that threshold effects only weakly worked against the initial hazard rate at small times and weakly aided the increase in hazard rate at large times.

4 | DISCUSSION AND CONCLUSIONS

The above analysis greatly extends time-to-failure predictions by including the crack-velocity threshold. The profound effect of the threshold is to restrict kinetic effects and thus restrict time-to-failure predictions to a finite applied-stress domain or crack-length domain by including a natural stress or crack-length lower bound. The lower bound characterizes reactive equilibrium analogous to the inert equilibrium upper bound and introduces a minimum stress for failure if crack length is specified (Figures 1, 2, 3A, and 4), and a minimum crack length if stress is specified (Figures 3B and 5C). This minimum bound greatly alters lifetime and reliability approaches relative to unbounded crack-velocity descriptions (Appendices 1 and 2).

Perhaps, a surprising result of the analysis is that threshold-proximity effects are weak, especially for crack-length-based failure predictions (Figures 1-4). There was very little deviation from the kinetically limited asymptotic lifetime responses as the threshold was approached, and, in fact, the inert equilibrium proximity effects were greater. Threshold effects on failure time are real and greatly affect design considerations as loading a cracked component at less than the threshold eliminates the possibility of failure. However, once the threshold is exceeded by any significant amount, failure times can be predicted using kinetically limited analyses alone, although this is an overly conservative design approach.

Threshold and threshold-proximity effects are greatly in evidence in constant stressing-rate (sometimes called dynamic fatigue) tests, however.[5] In these tests, the stress is increased from 0 at constant rate, $\dot{\sigma}_D$, until component failure at the strength, σ_D, or the conjugate failure time, t_D. The explanation of these observations in terms of the current analysis is that much of the failure time in constant stressing-rate loading is subthreshold with zero crack propagation. Equation 8b is revised for constant stressing rate to read,

$$\Sigma = \frac{\psi^2 \dot{\sigma}_D^2 t^2}{E^*}, \tag{29}$$

and reactive equilibrium is, thus, not achieved for stagnant period t_0 after the beginning of loading, where

$$\frac{\psi^2 \dot{\sigma}_D^2 t_0^2 c_0}{E^*} = 2\gamma. \tag{30}$$

For t just exceeding t_0, v is very small as G just exceeds 2γ. Hence, threshold-proximity effects are large in constant stressing-rate loading as t_D is extended by a stagnation period and crack propagation must begin from the threshold. Neither of these factors pertain to constant stress loading, and hence, threshold-proximity effects are small in this case.

Another perhaps surprising result is that temperature effects on the crack-velocity response are small, Figure 2, suggesting the temperature effects in time-to-failure and reliability predictions will be small. This result is at odds with industrial practice in which temperature excursions are used in aging studies to arrive at "acceleration factors" for empirical reliability predictions.[15] The resolution to this difference is that stress effects on time-to-failure and hence reliability predictions are large (Figure 2). Hence, if the uniform, component-scale applied stress and the temperature are coupled through a coefficient of thermal expansion (CTE) effect, the stress changes could be large and hence the effects of temperature changes could be large. Modifying Equation 8b as

$$\Sigma = \frac{\psi^2 [\sigma_A + E^* \Delta\alpha(T - T_{ref})]^2}{E^*}. \tag{31}$$

gives the effect, where $\Delta\alpha$ is the CTE mismatch between a ceramic component and its surroundings and T_{ref} is a reference temperature at which CTE effects are zero. Depending on the relative signs of $\Delta\alpha$ and $(T - T_{ref})$ and whether the product $\Delta\alpha(T - T_{ref})$ is positive or negative, temperature effects may aid or oppose applied stress effects and thermal activation kinetics, and hence, no general statement can be made about the effects of temperature on brittle component reliability, other than the effects are probably not dominated by thermally activated kinetics changes (Figure 2D). An athermal uniform stress, σ_S, perhaps associated with manufacturing surface finishing such as machining or ion milling may preexist in the component, leading to further modification of Equations 8b and 31 as follows:

$$\Sigma = \frac{\psi^2 [\sigma_A + E^* \Delta\alpha(T - T_{ref}) + \sigma_S]^2}{E^*}. \tag{32}$$

Again, depending on the sign of σ_S, preexisting stress effects may aid or oppose the applied stress, decreasing or increasing reliability.

Nonuniform athermal stresses, perhaps associated with shock, particle contact damage, or microstructural effects, may also preexist in the component, and reliability predictions can be made by modifying Equation 8a as[4,5]

$$G = [(\Sigma c)^{1/2} + g_1(c,t)^{1/2} + g_2(c,t)^{1/2} + g_3(c,t)^{1/2} + \ldots]^2. \tag{33}$$

The first term on the right side in Equation 33 encapsulates Equations 29 and 32 and the remaining terms, $g_i(c, t)$, describe nonuniform stress effects. Of great importance is $g \sim c^{-3}$ for contact flaws, aiding crack propagation, decreasing with crack length, and pervasive in ceramics, glasses, and other brittle materials.[4,5] Analytical lifetime solutions including contact effects exist for assumed power-law crack velocities.[16] Additionally important are microstructural effects, typically varying as $g \sim -(1 - c^{-X})$ (with $X > 1$), written to reflect a resistance to crack propagation that depends on microstructure and increases with crack length to a steady-state value (an R-curve).[3–5,17] R-curve effects are usually absent in fine-grain ceramics and glasses and mostly evident in large-grain polycrystals and phase transforming ceramics, greatly affecting lifetimes and measured or deconvoluted crack velocities.[3–5,17] As many R-curves derive from microstructural-scale stress distributions coupled to crystallographic CTE inhomogeneity, temperature changes could affect lifetimes through variable crack resistance effects. Prior crack propagation or damage, such as occurs in cyclic fatigue, can also modify fracture resistance, especially the threshold[18] and thereby also affect lifetime. In any event, a large, but surmountable, practical difference exists between Equations 32 and 33 for reliability predictions in that Equation 32 leads to analytical

solutions, as here, and Equation 33 (and $B(c)$) requires numerical integration, as shown earlier.[5] (Equations 12a, 13a, and 17 must also be modified.[5])

Nonuniform applied stresses can also be described by Equation 33. Such stresses arise if a component is an odd shape, or the crack is long relative to the component, or extends to perturb the stress field, or changes with time.[19] If the applied stress is the only crack propagation force, it is convenient, however, to re-cast the problem with all terms $g = 0$ in Equation 33 and set crack-length dependent $\psi = \psi(c)$ in Equation 8b and thence the first term in Equation 33. Analytical solution is then usually precluded and numerical solution is required. Attention is then also focused on crack propagation and its effects rather than on component structural failure and reliability. Examples include crack propagation in semiconductor structures in which fracture and delamination can cause electrical failure but not structural failure;[20] crack propagation in dental structures in which fracture can lead to chemical contamination and chipping but not tooth failure;[21] and crack propagation in fire-affected concrete beams in which fracture leads to increased compliance and deflection but not beam failure.[22] In the last 2 examples,[21,22] extended finite element analysis was used to calculate the crack driving force and path as fracture perturbed the stress field in the irregular component; this will usually be required for complicated engineering structures.

In addressing long-term reliability including threshold effects, it is important to place the current work in context. A recent work[5] considered the kinetically limited strengths of a range of ceramics, including contact-flaw stress relaxation, microstructural toughening, and a threshold in the crack-velocity function, all while under constant stressing-rate loading. Unsurprisingly, the complicating factors required numerical solutions for strength predictions. A subsequent experimental work[19] omitted microstructural effects and showed that constant stressing-rate loading and long-term zero-stress aging in moderately corrosive environments could significantly affect reliability predictions through flaw alteration effects. Another work[23] simplified consideration even further by omitting all effects of microstructure, contact-flaw alteration, and crack-velocity thresholds, to demonstrate a method for short-term reliability prediction in reactive environments for components under constant applied stress containing contact flaws. In the work here, different simplifications are made to arrive at long-term analytical reliability predictions: Microstructural effects and contact-flaw stress fields are omitted, components containing simple cracks under constant applied stress are considered, but the crack-velocity threshold in the reactive environment is included. In addition, the works cited[5,19,23] made deterministic reliability predictions as only mean responses were considered. Here, probabilistic reliability predictions are made as the distribution of responses is considered.

Finally, it is important to note that the new ideas introduced here—incorporation of crack-velocity thresholds into time-to-failure predictions and extension of time-to-failure responses into reliability and hazard predictions—are based on underlying physical principles. A clear physical development exists[2,6] linking thermally activated bond-rupture processes to macroscopic crack-velocity behavior—the crack-velocity curve was not just taken as given and time-to-failure calculated. Similarly, a clear physical linkage was developed between a population of cracks and the conjugate variation in lifetime—the lifetime was not just taken as given as a function of applied stress and the reliability then calculated. In both cases, the underlying length scale is much smaller than the required design property. Nanoscale bond-rupture time scales are much smaller than time-to-failure of a macroscopic component. Micro-scale relative crack length extension rates are much smaller than the hazard rate of a population of components.

ORCID

Robert F. Cook http://orcid.org/0000-0003-0422-8881

REFERENCES

1. Lathabai S, Rödel J, Dabbs T, Lawn BR. Fracture mechanics model for subthreshold indentation flaws Part II Non-equilibrium failure. J Mater Sci. 1991;26:2313–21.
2. Cook RF, Liniger EG. Kinetics of indentation cracking in glass. J Am Ceram Soc. 1993;76:1096–105.
3. Chevalier J, Fantozzi G. Slow crack propagation in ceramics at the nano- and micro-scale: effect of the microstructure. In: Bradt RC, Munz D, Sakai M, White KW, editors. _Fracture Mechanics of Ceramics_. New York, NY: Springer Science+Business Media Inc; 2005: p. 173–90.
4. Lathabai S, Lawn BR. Fatigue limits in noncyclic loading of ceramics with crack-resistance curves. J Mater Sci. 1989;24:4298–306.
5. Cook RF. Multi-scale effects in the strength of ceramics. J Am Ceram Soc. 2015;98:2933–47.
6. Lawn BR. An atomistic model of kinetic crack growth in brittle solids. J Mater Sci. 1975;10:469–80.
7. Kurtz SK, Levinson S, Shi D. Infant mortality, freaks, and wear-out: application of modern semiconductor reliability methods to ceramic multilayer capacitors. J Am Ceram Soc. 1989;72:2223–33.
8. Walpole RE, Myers RH. _Probability and Statistics for Engineers and Scientists_. New York, NY: Macmillan Publishing Company Inc; 1972.
9. Klutke G-A, Kiessler PC, Wortman MA. A critical look at the bathtub curve. IEEE Trans Reliab. 2003;52:125–9.
10. Rice JR. Thermodynamics of the quasi-static growth of Griffith cracks. J Mech Phys Solids. 1978;26:61–78.
11. Cook RF. Effective-medium theory for the fracture of fractal porous media. Phys Rev B. 1989;39:2811–4.
12. Griffith AA. The phenomena of rupture and flow in solids. Phil Trans R Soc Lond A. 1921;221:163–98.

13. Orowan E. The fatigue of glass under stress. Nature. 1944;154:341–3.

14. Fett T, Munz D. Methods of determining subcritical crack growth by static lifetime tests with natural and artificial cracks. J Test Eval. 1991;19:461–6.

15. Hartzell AL, da Silva MG, Shea HR. *MEMS Reliability*. New York, NY: Springer; 2011.

16. Fuller ER Jr, Lawn BR, Cook RF. Theory of fatigue for brittle flaws originating from residual stress concentrations. J Am Ceram Soc. 1983;66:314–21.

17. Härtelt M, Fünfschilling S, Schwind T, Riesch-Oppermann H, Fett T, Kruzic JJ. Deducing the fatigue crack growth rates of natural flaws in silicon nitride ceramics: role of *R*-curves. J Am Ceram Soc. 2013;96:2593–7.

18. Kruzic JJ, Cannon RM, Ager JW III, Ritchie RO. Fatigue threshold R-curves for predicting reliability of ceramics under cyclic loading. Acta Mater. 2005;53:2595–605.

19. Cook RF. Strength of brittle materials in moderately corrosive environments. J Am Ceram Soc. 2018;101:1684–95.

20. Cook RF, Thurn J. Stable dielectric fracture at interconnects from electromigration stresses. Acta Mater. 2002;50:2627–37.

21. Barani A, Chai H, Lawn BR, Bush MB. Mechanics analysis of molar tooth splitting. Acta Biomater. 2015;15:237–43.

22. Liao F, Huang Z. Modeling cracks of reinforced concrete slabs under fire conditions. J Struct Eng. 2018;144:04018030.

23. Cook RF. A simple method of short-term mechanical reliability predictions for ceramics in reactive environments, online. J Am Ceram Soc. 2018;101:2727–31. https://doi.org/10.1111/jace.15526.

24. Hillig WB. The C-H delayed failure mechanism revisited. Int J Fracture. 2006;139:197–211.

25. Hertzberg RW. *Deformation and Fracture Mechanics of Engineering Materials*, 3rd ed. New York, NY: John Wiley and Sons; 1989.

26. Cook RF. Theory of time-dependent failure for fractal porous aggregates. In: Boland JN, Fitz Gerald JD, editors. *Defects and Processes in the Solid State: Geoscience Applications, The McLaren Volume*. Amsterdam, The Netherlands: Elsevier Science Publishers, B.V; 1993: p. 229–42.

APPENDIX 1

CORROSION-BASED CRACK-VELOCITY EXPRESSIONS

The lifetime analyses here and their underlying crack-velocity formulation focus on the stress part of stress-corrosion cracking. In this view, planes of interatomic bonds are sequentially ruptured, leading to a crack advance in which ruptured bonds decrease energy through reaction with environmental species.[6] The bond-rupture process is biased in the forward direction by a tensile stress—mechanical energy in the system is decreased, and surface energy increased, by crack advance. A balance between the changes of these 2 energies with crack length, characterized by G and 2γ, respectively, defines a zero in the net configurational force on the system—equilibrium—and a consequent zero in the crack velocity. An overbalance of 2γ by G (either increasing the applied stress or the reactivity of the environment) leads to a positive crack velocity, and it is then the integrated effects of the $v(G)$ and $G(c)$ dependencies that determine lifetime. Lifetimes diverge for values of G approaching the threshold 2γ, at which these configurational forces are equal.

A very different picture of lifetimes emerges, however, for analyses focusing on the *corrosion* aspects of stress corrosion. In these formulations, it is the relative *rates* of chemical *reactions* that determines crack-velocity behavior, rather than the relative *magnitudes* of physical *forces*. In this somewhat older view,[24] material is literally removed from the solid at the crack tip as a consequence of reaction with the environmental species. Chemical potential energy is decreased and surface energy increased by crack advance. The reaction rate is enhanced above that occurring on a flat surface of the solid by tensile stresses concentrated at the crack tip. Lifetimes are thence determined by the dependence of the corrosion rate on the crack-tip stress, which, in turn, depends on the crack-tip configuration. Divergence in the lifetime occurs for a fixed crack-tip configuration and a corrosion rate equal to that of the solid surface. The threshold in this case arises at a *kinetic steady-state* at the equality of 2 rates, rather than at a *thermodynamic equilibrium* at the equality of 2 forces.

Lifetime vs applied stress predictions from the kinetic view bear strong similarity to the sigmoidal curves generated, here, in Figures 1-3. However, as might be expected, there are very different connections between the macroscopic crack propagation parameters and underlying atomistic reaction parameters in the 2 views, with subsequent differences in lifetime dependencies. These differences are conveniently examined by casting both crack-velocity formulations into a thermodynamic framework. Both views start with the concept that the rate of change of a macroscopic variable Y is the product of a frequency f_0 modified by Arrhenius terms and a minimum variable "step-size" Y_{min}:

$$\dot{Y} = f_0 \left[\exp\left(\frac{-U_+^*}{kT}\right) - \exp\left(\frac{-U_-^*}{kT}\right) \right] \times Y_{min}, \quad (A1)$$

where $U_\pm^*$ are the activation barriers for forward and backward minimum steps. The first and largest difference between the 2 views comes in the choice of the macroscopic variable: in the "stress" view, as here, the cracked area $Y = A$ is used; in the "corrosion" view, the removed volume $Y = V$ is chosen. As a consequence, the conjugate configurational force y differs. This force is defined by

$$y = -\frac{dU}{dY}, \tag{A2}$$

where U is the total internal energy of the system. For the stress view, the configurational force $y = (G - 2\gamma)$, the global energy release rate. For the corrosion view, the configurational force is chosen as $y = \sigma_t$, the crack-tip stress.

The dependence of $U_\pm^*$ on y is determined by expanding the barrier height to first order about the value u_1 at $y = 0$ (noting that this condition defines equilibrium for the stress view but not for the corrosion view):

$$U_\pm^* = u_1 \mp \left(\frac{\partial U_\pm^*}{\partial y}\right)_{y=0} y \pm \dots, \tag{A3}$$

where the $\mp$ sign indicates that positive forces decrease the barrier. The stress analysis used here sets $\partial U_\pm^* / \partial(G - 2\gamma) = a^2$ and the rest of the analysis follows. The corrosion analysis interprets $\partial U_\pm^* / \partial \sigma_t = V^*$ as an activation volume and sets $V^* = V_{min}$. However, before developing a crack-velocity formulation, this analysis includes 2 somewhat counteracting modifications to the $U_\pm^*$ values used in Equation A1: The second term characterizing the frequency of backward reaction is neglected, essentially setting $U_-^* = \infty$, and the forward barrier height U_+^* is modified to represent the total energy change for an incremental step, ΔU, such that the frequency term in Equation A1 becomes $f_0\exp(-\Delta U/kT)$. ΔU is given by adding a term to U_+^* representing the energy required to create new surface. In the notation here,

$$\Delta U = u_1 - \sigma_t V^* + u_0. \tag{A4}$$

The first term in Equation A4 is interpreted as the intrinsic energy barrier to V_{min} removal on a flat surface. The third term adds to this barrier the energy required to create new surface at a crack tip and is often written as $\gamma V_{min}/\rho$ where ρ is a crack-tip radius. The second term decreases the barrier and drives the corrosion process at the crack tip through a stress concentration, $\sigma_t = \sigma_A[1 + (c/\rho)^{1/2}]$. Later analyses represented the enhanced crack-tip stress by a stress-intensity factor K, $\sigma_t = 2K/(\pi\rho)^{1/2}$, such that the rate of volume removal at the crack tip is

$$\dot{V} = \dot{V}_0\exp\left[\frac{(b\sigma_A - E^*)}{kT}\right], \tag{A5}$$

and by implication the crack velocity is[17]

$$v = v_0\exp\left[\frac{(bK - E^*)}{kT}\right]. \tag{A6}$$

The $\dot{V}_0$ and v_0 terms characterize intrinsic corrosion or crack propagation rates and involve terms of $\exp(-u_1/kT)$. The b term characterizes the enhancement of the corrosion or crack propagation rates by the crack-tip stress and has a $\rho^{-1/2}$ dependence. The E^* term characterizes the impediment of the corrosion or crack propagation rates by the work required to generate new surface and has a γ/ρ dependence.

Equation A6 can be used to describe a lot of crack-velocity measurements—particularly over limited ranges of K—and can be integrated easily to obtain lifetimes; Equation A6 bears some resemblance to Equation 6. Problems arise, however, in the extension of the thermally activated corrosion analysis to an analogous crack-propagation analysis—particularly with respect to the threshold. The $\dot{V}_0$ term in Equation A5 is interpreted as the rate of material removal on a flat surface. For a balance at the crack tip such that the enhanced reaction rate caused by the stress just balances the diminished rate caused by the creation of highly curved surface, the crack tip advances no more rapidly than the surface and the crack-tip configuration, characterized by ρ, does not change. The stress $\sigma_{min} = E^*/b$ at which this steady-state topography condition occurs was interpreted as the lower bound to the stress necessary to cause stress-corrosion cracking and the lifetime, defined by the integrated motion of the crack tip relative to the surface, diverges at this stress. For a similar balance in the arguments of the exponential term in Equation A6, however, the crack velocity does not vanish: v_0 is simply a scaling factor; at $K = E^*/b$, $v = v_0$. Even for $K = 0$, v is nonzero. Thresholds could easily be mathematically inserted in corrosion-based crack-velocity formulations and fit to existing crack-velocity and lifetime data. However, the original underlying concept of a propagating "notch" at which material is removed on a characteristic scale ρ and to which the reactive environment has full access conflicts with more recent observations and models of crack profiles.[5] In addition, this concept sets up an artificial distinction between crack propagation in reactive environments (notch propagation) and that in inert environments (bond breaking) by choosing volume rather than area as the extensive variable and thereby breaks consistency with the Griffith concept. Hence, although it is possible to re-work the corrosion model to generate a crack-velocity formulation, the concept of bond rupture rather than atom removal retains superiority for lifetime prediction.

APPENDIX 2

LIFETIME SOLUTIONS FOR POWER-LAW CRACK-VELOCITY APPROXIMATION

Crack-velocity behavior is often approximated by a power-law dependence on the driving force for fracture. The Paris law description of cyclic fatigue behavior in metals and polymers[25] is $dc/dN \sim (\Delta K)^n$, where ΔK is the amplitude of the cyclic stress-intensity factor variation and N is cycle number. This is often extended to describe noncyclic loading behavior of ceramics by $v = dc/dt = AK^n$, where A and n are empirical. Some analytic simplicity is achieved using these approximations due to the power-law function and the lack of a threshold.[16]

A power-law approximation to the crack velocity that retains the threshold is

$$v = v_0[(G - 2\gamma)/\eta]^n/B, \qquad (A7)$$

analogous to Equation 5, and which in the limit of $G \gg 2\gamma$ becomes

$$v = v_0(G/\eta)^n/B, \qquad (A8)$$

analogous to Equation 6, noting that this has the same functional dependence as the Paris laws above. Using Equation 9 to define G yields the crack-extension integral as follows:

$$t_c = \int_{c_0}^{c} \frac{dc'}{v_0[(G - 2\gamma)/\eta]^n/B}, \qquad (A9)$$

analogous to Equation 10. Changing variables using Equation 11 gives the solution to Equation A9:

$$t_c = \frac{\eta B}{\Sigma v_0(n-1)} \left[z_0^{-(n-1)} - z^{-(n-1)} \right], \qquad (A10)$$

analogous to Equation 12. Defining Orowan limits as per Equations 13 and 14, and using the normalizations of Equation 15 yields the time for crack extension under applied stress from Equation A10 as

$$T_C = \frac{B}{WS^2(n-1)} \left\{ [W(S^2 - 1)]^{-(n-1)} - [W(S^2C - 1)]^{-(n-1)} \right\}, \qquad (A11)$$

analogous to Equation 16a. Setting Griffith limits of Equations 17 and 18 yields the failure time analogous to Equation 19:

$$T_f = \frac{B}{WS^2(n-1)} \left\{ [W(S^2 - 1)]^{-(n-1)} - [W(S_{max}^2 - 1)]^{-(n-1)} \right\}, \qquad (A12)$$

with the same bounding asymptotic limits and an intermediate asymptote of,

$$T_f \to \frac{BW^{-n}S^{-2n}}{(n-1)}, \qquad (A13)$$

obtained by integrating Equation A8 directly.[16] Similar solutions have been presented for nonconstant fracture resistance $2\gamma (c/\delta)^d$ replacing 2γ in Equation A7.[26]